INTL JOURNAL OF ELECTRONICS AND TELECOMMUNICATIONS, 2010, VOL. 56, NO. 3, PP. 223-230
Manuscript received July 10, 2010: revised September, 2010. DOI: 10.2478/v10177-010-0029-9

Readout System and Data Processing for OCT Pachymetry

Michał Dziewiecki, Grzegorz Domański, Wojciech Frey, Bogumił Konarzewski, Robert Kurjata, Janusz Marzec, Andrzej Smolnik, Krzysztof Zaremba, and Marcin Ziembicki

***Abstract*—A complete system for measurement control, signal acquisition and data processing for an OCT pachymeter is described. Moreover, dedicated data processing algorithm used for noise reduction is presented. A simple OCT scanner was built and some measurements were performed to examine the capabilities of the system.**

***Keywords*—Optical coherence tomography, pachymetry, optical signal detection.**

I. Introduction

CORNEAL PACHYMETRY is a medical diagnostic method giving information on cornea thickness. Pachymetry is used in glaucoma diagnosis, being a supplementary examination to applanation tonometry, where cornea thickness is an important factor affecting measured interocular pressure. Pachymetry is also used in corneal surgery methods such as LASIK (Laser-Assisted in situ Keratomileusis), LRI (Limbal Relaxing Incisions) and others to observe patient's cornea shape.

Depending on measurement technique used, pachymetry can be realized as contact measurement (e.g. ultrasound thickness measurement) or noncontact one (various optical methods).

One of the most promising non-contact methods is the Optical Coherence Tomography (OCT)[1], as it achieves very high accuracy (≈1 μm), provides a very well defined measurement position over the cornea region and is easy to automate. Last but not least, the same method can be used for measurement of deeper eye structures position (biometry). A short comparison of ultrasound and OCT techniques can be found in [5].

An example of cornea scan is presented in figure 1.

II. OCT Pachymetry Basics

A. Time-Domain Optical Coherence Tomography

Figure 2 shows a Michelson interferometer, which can be used as a basic type of a time-domain OCT free-space device. (An alternative for the free-space solutions are optical fibre based devices). The main difference between OCT scanner and a classic interferometer is that one of the mirrors is replaced by measured sample. Furthermore, specific light sources with low light coherency are used, such as superluminescent diode (S-LED), femtosecond laser, LED or (rarely) thermal source.

The beam of the light source is divided into two separate paths in the splitter. One of the resultant beams is reflected by a moving reference mirror (this is the reference arm of the device) and the other by scanned object (the measurement arm). Both beams are then mixed together by the same beam splitter and directed into the light detector (in most cases a photodiode). The moving mirror provides depth scan (z-axis scan) of the object and allows for generation of interference

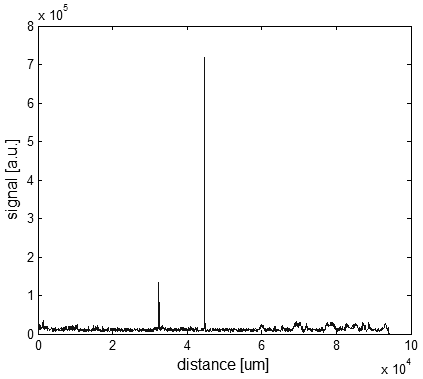

Fig. 1. An OCT scan of swine cornea obtained by Authors. The right peak represents external cornea surface and the left one stands for its inner bound.

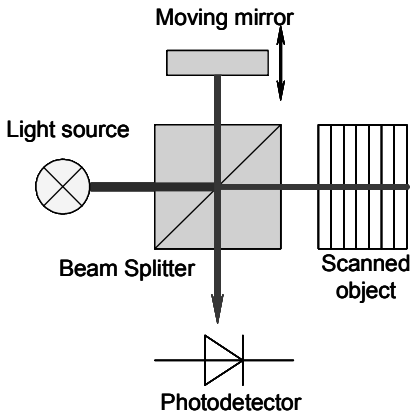

Fig. 2. A schematic of the Time-domain OCT system. Moving mirror provides the depth scan.

M. Dziewiecki, G. Domański, B. Konarzewski, R. Kurjata, J. Marzec, A. Smolnik, K. Zaremba, and M. Ziembicki are with Warsaw University of Technology, Institute of Radioelectronics, Nowowiejska 15/19, 00-665 Warsaw, Poland (e-mail: {M.Dziewiecki; G.Domanski; B.Konarzewski; R.Kurjata; J.Marzec; A.Smolnik; K.Zaremba; M.Ziembicki}@ire.pw.edu.pl).

W. Frey is with Frey S.J., Wołodyjowskiego 38, 05-502 Piaseczno, Poland (e-mail: wojciech@frey.pl).

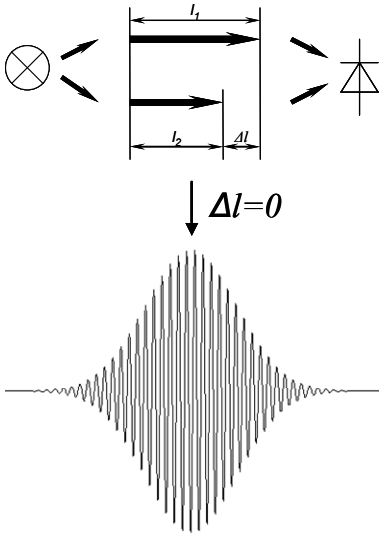

Fig. 3. Interference signal from a single reflecting surface.

signal. The x-y scan, if needed, can be performed by moving the apparatus across scanned object or by adequate optical system, changing beam position. Also, full-field devices are known, where single photodetector is replaced by multi-pixel structure such as CCD, allowing a full image scan in one measurement [2][4].

When the difference between both interferometer paths changes constantly (i.e. during mirror movement), an AC signal is generated on the detector. It can be divided into two components. The first one is a sum of light intensities from both interferometer paths and varies slowly with the mirror movement. It carries no information about the object and is not used in OCT. The second one is an interference component, which contains information about structure of examined object [1].

For an object consisting of only one light reflecting surface (such as a mirror), the interference signal has a form of a modulated pulse. The signal amplitude reaches highest value when optical length difference between both interferometer paths reaches zero (see fig. 3)

For an object, which can be modeled as a set of surfaces, where each surface represents material's refractive index discontinuity, each of them gives one pulse in the signal. The length of a single pulse is determined by lightwave's coherence length. A typical value is 50 μm for most commonly used superluminescent diodes. Generally, light's coherence length determines the depth (Z-axis) resolution of the OCT.

B. OCT Setup and Requirements for Corneal Pachymetry

Few further requirements must be taken into account when using OCT for pachymetry:

1) Scanning Depth

Scanned tissues are relatively thick for common OCT. The width of the cornea is typically only 1 mm, but the scanning range should be much wider, so that initial distance between the eye and the scanner doesn't need to be set accurately. Furthermore, wide scanning range provides an ability to scan deeper eye structures. Practically, scan depth of 10 mm should be provided.

Such range is hard to achieve with very popular Fourier-domain OCT, as it requires a very high resolution of the spectrometer. This limitation doesn't exist for time-domain technique. The only problem can be the light absorption in the tissue, but in the case of transparent eye structures it's not significant.

The main disadvantage of time-domain OCT in relation to Fourier-domain OCT is the scanning speed. In pachymetry, where only single measurements are performed, this issue has only a minor importance.

2) Depth Resolution

The theoretical resolution of ca 50 μm is generally too poor for pachymetry. However, in a case where individual reflecting layers are far away from each other, the signals generated by each layer are well separated. This means, that the position of each signal peak can be recognized with much higher accuracy than its FWHM. This way, a position readout accuracy of single micrometers can be reached when signal quality is sufficient.

3) Signal Dynamics

The output signal level is very dependent on incident angle of the light. For angles close to zero, the reflected beam gives a very good signal. But a deviation of only a few degrees can cause that the reflected beam doesn't reach the photodetector. In such case only a diffuse backscattered light is detected, giving relatively low signal. As result, high dynamic range of the readout system is desired to cover both high and low signal level from reflected and diffuse light.

III. EXPERIMENTAL DEVICE

A simple OCT device for pachymetry was built for experimental purposes. It provides single scans of artificial and in-vitro samples. Scanning of human eye is possible by the scanner itself, but its mount doesn't allow to place it in front of human's head. A simplified schematics of the device is presented in fig. 4.

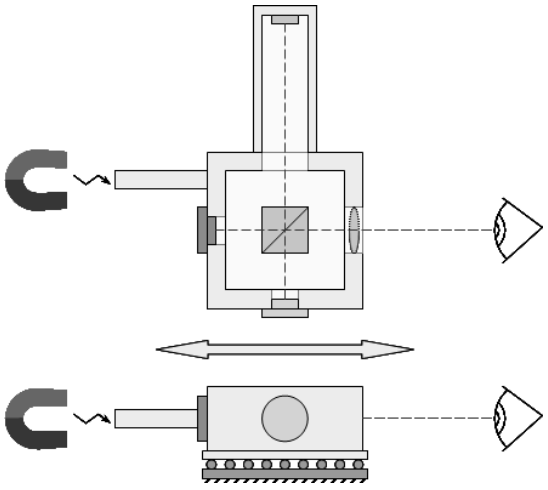

Fig. 4. Experimental pachymeter. Side view shows ball bearing. Magnetic drive is shown schematically.

In comparison to the model presented in fig. 2, the optical distance change is realized in the measurement arm instead of the reference one. The light source, detector, cubic beam splitter and the reference mirror are mounted within one rigid construction, which is moving back and forth on linear ball bearings. The movement of the whole scanner causes distance change between the beam splitter and measured sample, thus changing the measurement arm length. Such solution enables better beam focusing on scanned object, independently of initial scanner-sample distance.

The working movement of the scanner is realized using a solenoid while a set of permanent magnets provides the return movement. To check the actual position of the scanner, an optical linear encoder is used, providing theoretical position resolution of 1 μm.

The optical path of the device can be configured in several ways, including convergent and parallel beams and different types of light sources. For the experiments, two light sources were used:

- a Hamamatsu L8414-41 superluminescent diode (central wavelength λ_p=830 nm, spectrum width $\Delta\lambda$=15 nm FWHM, P_{opt}=5 mW) - for experiments with convergent beam
- an Exalos EBS-4000 broadband light source with single-mode fibre output (λ_p=830 nm, $\Delta\lambda$=90 nm). A high spectrum width is achieved by assembling several S-LEDs in one housing with common light output. For such technology, the spectrum is no more Gaussian-shaped, like it was for single S-LED. This light source was used together with single-mode fibre link and collimator in parallel beam experiments, where the beam was focused on scanned object by a single lens only. Convergent beam experiments were also performed with this source to compare with single S-LED.

IV. The Electronic Readout System

A. Main Functions and Subsystems

The readout system is responsible for OCT signal conditioning and acquisition, scanner position recording, measurement control and acquired data processing. It also provides user interface for measurement triggering and results visualization.

A block diagram of whole device is shown in fig. 5.

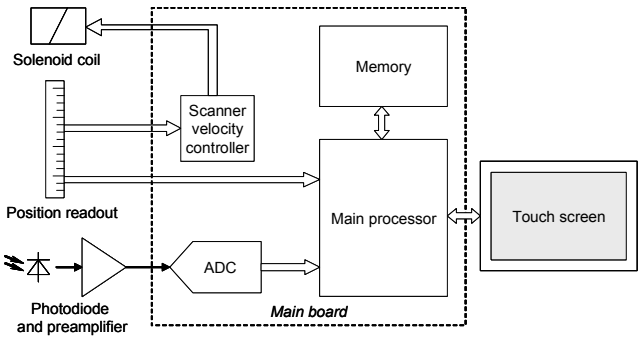

Fig. 5. Block diagram of the electronic readout and control system. Some minor subsystems are missed.

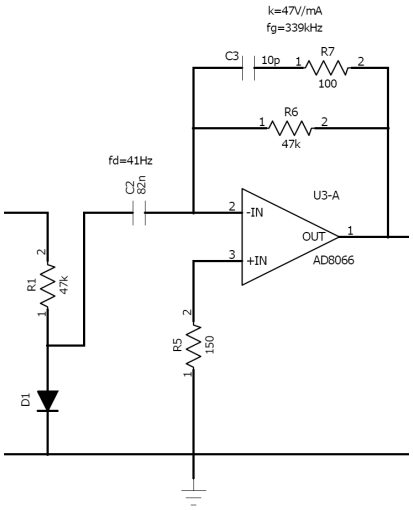

Fig. 6. First preamplifier stage. The photodiode is powered from a negative voltage source (not shown).

During a measurement, the signal from the photodiode is amplified and conditioned in a multi-stage preamplifier. Then it's transmitted to the ADC to be digitized and is stored in memory by the main processor. In parallel, actual scanner position is registered using an optical sensor. The position readout is also used to drive scanner's magnetic gear, providing relatively constant velocity of the scanner.

Main blocks of the device are described below.

B. Analog Front-End

The analog front-end circuitry consists of the photodiode and the preamplifier for signal conditioning.

For a photodiode, a Hamamatsu S1336-18BQ model was chosen due to low dark noise and low capacitance (thanks to small active area - 1.1 x 1.1 mm^2). Its sensitivity reaches 0.45 A/W for λ=830 nm. Maximum reverse voltage for this type is 5 V.

The preamplifier is fully based on operational amplifiers. Its first stage is presented in figure 6. The photodiode is polarized to a reverse voltage from a -4.7 V source to work in current mode. A three-stage RC ladder is used to filter the supply voltage. The amplifier works in current/voltage transducer configuration, giving very low input impedance for AC component of the photodiode current. The DC component is rejected from the output signal. A maximum constant optical power of ca 200 μW can be applied before the saturation of the input stage occurs and the diode comes into the photovoltaic mode. For bigger power, the diode polarising resistor can be changed to a lower value, but it leads to the noise increase.

An Analog Devices AD8066 amplifier is used in the first stage. This BiFET device provides high bandwidth, high input resistance and very low noise .

To achieve total gain of 0.3 V/nA, two additional amplifier stages are provided with the voltage gain of 83 each. Moreover, each stage has a high-pass and low-pass filter, with cut-off frequencies of 8.8 kHz and 106 kHz, respectively. They provide final bandwidth shaping with pass band of 10 to

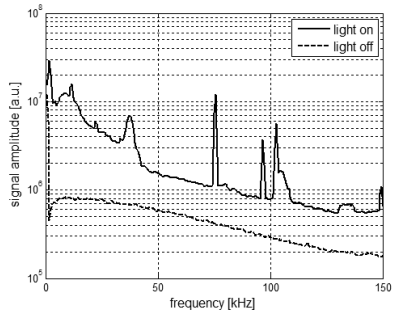

Fig. 7. Acquired signal spectrum during measurement with the S-LED light source turned on and off.

100 kHz. No additional anti-aliasing filter is used. Voltage amplifiers described above are built using a single NE5532 chip.

The noise figure of the whole amplifier is determined mostly by the photodiode shot noise coming from constant photocurrent, generated by DC component of light. It's shown in figure 7, that the overall noise level grows significantly when the light source is turned on. Furthermore, some peaks from OCT signal can be seen (they're placed on different frequencies due to scanner's velocity instability - see chapter V). Also, some low-frequency interference from the light source is visible.

High rejection rate of lower frequencies along with DC component rejection allows the device to work properly with every type of lighting in the room, including sunlight, bulbs and glow-tubes.

The preamplifier is installed next to the photodiode on the scanner box to avoid long conections and reduce the EMI influence.

C. ADC Converter and Main Processor

An Analog Devices AD7693 chip was used for signal digitalization. It's a 16-bit succesive aproximation ADC converter with serial output using an SPI bus. Its dynamic range exceeds 92 dB (including SNR and nonlinearities) for 100 kHz input signal frequency. The maximum sampling rate is 500 kHz, but for this application 300 kHz sampling was used.

The differential input of the ADC is driven by an ADA4941-1 driver from Analog Devices. A single-ended connection is used between preamplifier and the ADC driver.

The main processor of the system is a Freescale MCF5251 microcontroller. It's a midrange 32-bit device with 140 MHz Coldfire® core. Among other peripherals, it contains 128kB of static RAM memory, SDRAM controller, multi-purpose DMA controller and a set of external bus controllers, such as USB 2.0, ATA, CAN, I^2C, SP-DIF, UART and queued SPI.

To allocate data buffers, an external SDRAM memory with 4 MB capacity was added.

The scanner position measurement is realized directly by the microcontroller. The pulses coming from the linear encoder are counted (both slopes are taken into account) and the counter state is written down to memory together with every ADC sample.

Additional hardware connected to the main processor can provide further functionality including camera support for scanner targeting.

D. Scanner Velocity Controller

The magnetic drive gear used in experimental device does not ensure constant scanner velocity. During a free movement, it's rather growing rapidly than maintaining the same level. To provide a relatively invariant velocity, a special controller is used. It utilizes the signal from the position sensor and a phase-locked-loop (PLL) circuitry. The PLL drives the output solenoid to maintain relatively constant frequency of pulses coming from the position sensor. It allows keeping the velocity within ±30% limits.

E. User Interface

The user interface consists of an LCD screen with a touch panel. The screen is a color matrix with 320x240 points (QVGA) resolution. It incorporates a graphic controller with 16-bit memory-type interface to connect to the microprocessor. The controller provides constant screen refreshing, so the processor is involved only during picture change operations. Text generation is realized by software. The resistive touch panel provides user input. It's connected to main processor via an SPI link and operates independently from the graphic controller.

The user interface provides a number of operations, including measurement start, output signal view with zooming, automatic peak finding and distance measurement.

V. Signal Processing Algorithm

A. The Aim of Signal Processing

The shape of a single pulse, as it was shown in fig.3, is identical to used lightwave's autocorrelation function scaled in time by a factor of $^{c}/_{2v}$, where c denotes the speed of light and v is scanner velocity. The relative bandwidth of the pulse is dependent on relative bandwidth of used light source. As a typical S-LED diode has rather narrow spectral characteristics (15 nm FWHM, which gives 1.8% at mean wavelength of 830 nm), the output signal is supposed to be narrow-banded. This means, that band-pass filtering of the signal should strongly improve the signal to noise ratio when applied correctly. The problem is that center frequency of the signal is dependent on scanner velocity, which is controlled with relatively poor accuracy (see fig. 8).

To correct this problem, the information about scanner's position is used. If the signal is resampled from time domain to scanner position domain, its central frequency (now understood as spatial frequency) should be constant and dependent only on lightwave's central frequency. This enables easy filtering with a band-pass filter.

B. Signal Flow

As shown in fig. 9, the first stage of the signal flow is data acquisition. During a typical single 12-mm-deep scan about 80 thousands samples of OCT signal and position data are collected. They're stored in the SDRAM memory as 16-bit words.

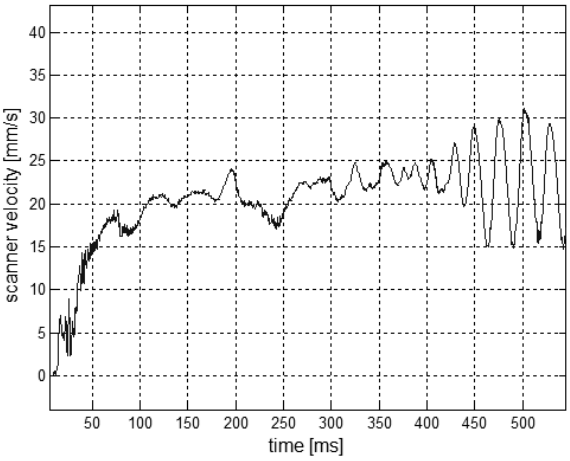

Fig. 8. Scanner velocity changes during measurement.

After scan completion the OCT signal is resampled using position information (the position is being smoothed before)

After signal resampling, a joint operation of filtering and amplitude detection is performed. The last action is peak detection. Two highest peaks are assumed to be cornea surfaces and the distance between them is calculated.

Key steps of data processing are described in following paragraphs.

C. Position Signal Smoothing

As the position readout device has resolution of 1 µm, which is poor in comparison to the wavelength of used light (830 nm) and additionally it has a quite big jitter (reaching approx. 0.5 µm), a position smoothing procedure is applied to get more accurate value at any given time. To perform this, a 1024-sample-long rectangle FIR filter is used. For rectangle filter response, only one addition and one subtraction must be performed for each signal sample, making this method very efficient.

The aim of this step is to reach position readout resolution of 125 nm. It gives the accuracy of almost ¼λ, which is enough for further processing (theoretically, ½λ is the limiting value to meet Nyquist requirements). The goal resolution can be changed by software if needed.

D. Signal Resampling

This step moves acquired OCT signal from time base to new spatial domain. To perform it, asynchronous sample rate conversion procedure (ASRC) is applied. New sample values are calculated for every position quantum (typically every 125 nm). To perform this, a *sinc*-type filter is used. The filter consists of 4096 samples (64 periods, 64 samples per period). The filter function is generated once and stored in microcontroller's internal SRAM memory to achieve possibly lowest access time. For each sample, 64 multiply-and-accumulate (MAC) operations must be performed. For one measurement, about 100 000 samples are to be calculated for 12 mm).

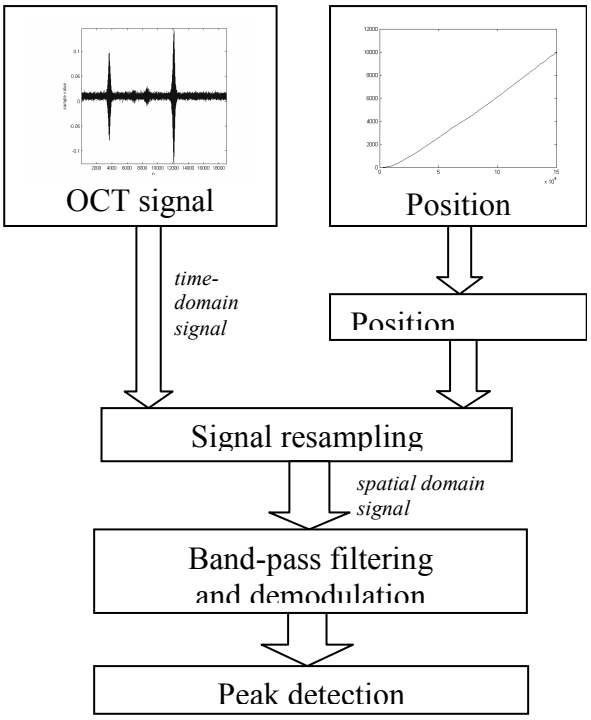

Fig. 9. Signal flow during data processing.

This is the most computational power consuming operation during signal processing. Some low-level optimizations were made to minimize calculation time. For a typical scan, this operation takes about two seconds.

E. Band-Pass Filtering and Demodulation

To perform the signal filtering procedure, a FIR filter with complex coefficients is used. It's shape should be matched to OCT signal's shape (fig. 3). In practice, a theoretically calculated filter was used. Its main form is:

$$w_n = e^{-\left(\frac{n \cdot Ts}{\sigma}\right)} \cdot e^{-j\,2\pi f_o \cdot T_s} \qquad (1)$$

where w_n denotes n^{th} sample of the filter pulse response, T_s is sampling period (in distance units), f_0 is central frequency of a single OCT pulse and σ is its width. The left component of the equation describes Gaussian envelope, while right one stands for modulating sine. Typically, 256-sample-long filter was used.

The use of complex filter coefficients simplifies signal amplitude detection, because the only operation to perform after convoluting input signal with the filter response is to get the absolute value for each complex sample.

Because calculating of the absolute value requires square root operation, which is computationally inefficient, a rough algorithm, being a derivative of so called $A_{max}B_{min}$ procedure [3] is used. It utlilizes simple linear formulas to estimate the absolute value of a number, distinguishing four cases:

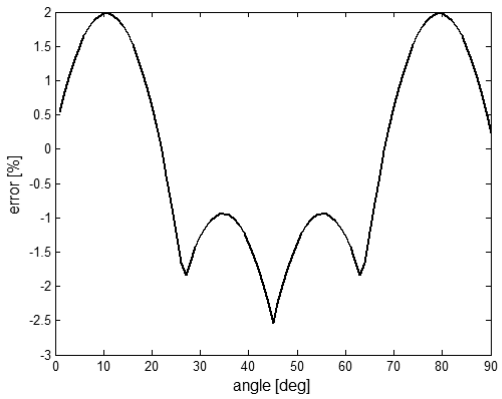

Fig. 10. Error of used absolute value estimation algorithm for arguments in first quarter of the coordinate system.

$$|X| = \begin{cases} H + \frac{3}{16}L & \Leftrightarrow \quad H \geq (2L) \\ \frac{13}{16}H + \frac{9}{16}L & \Leftrightarrow \quad (2L) > H \geq L \end{cases} \tag{2}$$

where:

$H = \max[re(X), im(X)]$,

$L = \min[re(X), im(X)]$.

The RMS error of used method is only 1.43%. Full error plot is shown in fig. 10.

The filtering and amplitude detection are performed with 1 µm step, giving final measurement resolution of 1 µm. Higher resolution is not required as the real measurement accuracy hardly ever maintains this level. Furthermore, living tissue like cornea changes its shape constantly (e.g. due to pressure variations in adjacent blood vessels) and measuring its dimensions with micrometer precision may be controversial.

F. Peak Detection

Last step of signal processing is detection of signal peaks which represent discontinuities in tissue structure (e.g. cornea edges). The detection level is automatically calculated basing on signal's histogram, so that most of the noise is rejected preserving possibly highest sensitivity. (By default, the detection level is set to be higher than 95% of signal samples after amplitude detection - see fig. 11). Exact peak height is calculated as an integrate of samples greater than detection level and its position as center of gravity.

Additionally, some artifacts can be removed basing on a fact, that a false peak looks like an echo of a real peak shifted by a known distance. This allows partial rejection of internal parasitic reflections in the structure of some cheaper S-LED devices. Nevertheless, applying this algorithm will cause detection efficiency loss in some regions of the scan, where artifacts are expected.

VI. RESULTS

A number of measurements were performed to check readout system's capabilities. The tests included noise rejection

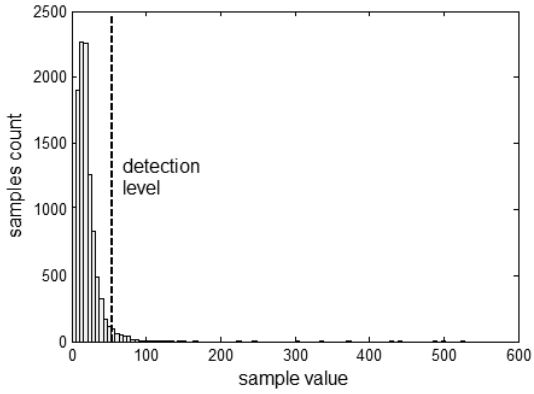

Fig. 11. Sample histogram after amplitude detection. Peak detection level is shown.

effectiveness, ability of working with very small signals and thickness measurement repeatability. For testing, artificial samples and in-vitro material (swine eye) were used. For all tests, the goal was to obtain best results from weak data rather than optical signal increase.

Figure 12 presents filtering algorithm capabilities. Using highly distorted light from the light source (both low- and high-frequency interference coming from the switching power supply of the EBS-4000 source) a high quality output signal is obtained.

The scan in fig.13 is acquired with bad sample arrangement – the swine eye is shifted perpendicular to scanning axis by about 0.5 mm, causing that reflected beam does not reach the photodiode. In this case, only weak diffuse reflection is observed. Despite scan quality loss, the cornea is still visible.

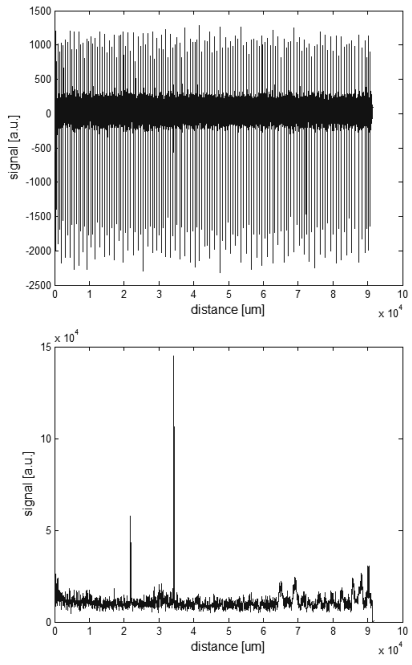

Fig. 12. OCT signal before (upper plot) and after (lower plot) the filtering and amplitude detection procedure. High interference background coming from light source power supply is rejected. The scan presents a swine cornea.

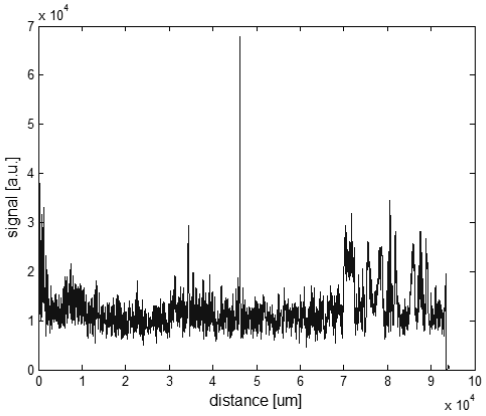

Fig. 13. Swine cornea scan using diffuse light with bad calibration of the optics. Both cornea surfaces are still visible.

The thickness measurement repeatability tests were performed using a flat glass sample (approx. 3 mm thick) as it surely maintains its dimensions during long measurement series. Figure 14 presents results for 113 consecutive measurements.

VII. Conclusions

The RMS error for this data was 1.26 µm. It must be noticed that measurement accuracy will deteriorate for bad signal quality.

A complete electronic system for OCT pachymeter was built. The device realizes all tasks from measurement control, through data acquisition and signal processing, to user's interface handling and results visualization.

The system is capable of useful data extraction even with low signal quality and big interference. Optical power AC component far below 100 pW can by detected, with further improvement given by signal processing techniques. Also, high interference immunity (both for optical and electrical signals) was achieved. Output waveforms are fairly resistant to saturation of the analog circuits in case of very high signals, with only moderate distortion in their shape.

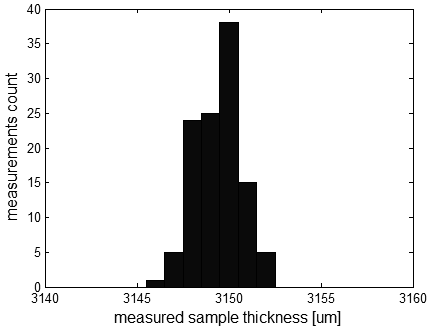

Fig. 14. Thickness measurement thickness histogram for 113 measurements.

Used data processing algorithms require relatively low computational power, enabling acceptable calculation times (2-5 s for single measurement, typically) using a midrange 32-bit microcontroller.

Some noise is added by constant point arithmetics used for calculations, but it's negligible in comparison to the noise in received signal.

References

[1] B. E. Bouma and G. J. Tearney, *Optical Coherence Tomography*. New York: Marcel Dekker Inc., 2002.

[2] S. Chang, X. Liu, X. Cai, and C.P. Grover, "Full-field coherence tomography and its application to multiple-layer 2D information retrieving," *Optics Communications*, no. 246, pp. 579–585, 2005.

[3] R. G. Lyons, *Understanding digital signal processing*. 2nd ed. Upper Saddle River NJ: Prentice Hall, 2004, pp. 400–406.

[4] T. Motoyama, K. Nitta, O. Matoba, and T. Yoshimura, "Study on Variable Resolution Imaging in a Microscope OCT System," in *Pacific Rim Conference on Lasers and Electro-Optics*, Tokyo, 2005, pp. 336–337.

[5] C. A. Puliafito et al., *Optical Coherence Tomography of Ocular Diseases.* Thorofare NJ: Slack Inc., 2004, pp. 1-16.